Simultaneous Prediction of Wrist and Hand Motions via Wearable Ultrasound Sensing for Natural Control of Hand Prostheses

Xingchen Yang, *Member, IEEE*, Yifan Liu, Zongtian Yin, Pu Wang, Peilin Deng, Zhengen Zhao, and Honghai Liu, *Fellow, IEEE*

***Abstract*— Simultaneous prediction of wrist and hand motions is essential for the natural interaction with hand prostheses. In this paper, we propose a novel multi-out Gaussian process (MOGP) model and a multi-task deep learning (MTDL) algorithm to achieve simultaneous prediction of wrist rotation (pronation/supination) and finger gestures for transradial amputees via a wearable ultrasound array. We target six finger gestures with concurrent wrist rotation in four transradial amputees. Results show that MOGP outperforms previously reported subclass discriminant analysis for both predictions of discrete finger gestures and continuous wrist rotation. Moreover, we find that MTDL has the potential to improve the accuracy of finger gesture prediction compared to MOGP and classification-specific deep learning, albeit at the expense of reducing the accuracy of wrist rotation prediction. Extended comparative analysis shows the superiority of ultrasound over surface electromyography. This paper prioritizes exploring the performance of wearable ultrasound on the simultaneous prediction of wrist and hand motions for transradial amputees, demonstrating the potential of ultrasound in future prosthetic control. Our ultrasound-based adaptive prosthetic control dataset (UltraPro) will be released to promote the development of the prosthetic community.**

***Index Terms*— Simultaneous wrist and hand motion control, transradial amputees, wearable ultrasound, multi-out Gaussian process, multi-task deep learning, UltraPro dataset.**

I. Introduction

THE lack of motor abilities, as well as self-perception issues and phantom limb pain, may affect the lives of individuals with transradial amputation in physical, emotional, and financial matters. Cosmetic prostheses can address appearance, but they cannot improve motor function. Current prosthetic hands, however, are now able to replicate most of the functions of the human hands while maintaining a natural appearance. Unfortunately, the complexity of controlling all of those degrees of freedom (DoFs) places an excessive cognitive burden on the user. Indeed, current human-prosthetic interfaces are usually limited to a non-intuitive, sequential and on/off control of a limited number of DoFs, which can only restore some simple hand functions. As natural hand movements are usually composed of simultaneous activation of wrist and hand motions, a biomimetic and intuitive controller of the prosthetic hand should be able to provide simultaneous control of multi-DoF wrist and hand movements.

There are mainly two types of methods to achieve simultaneous control of muti-DoF wrist and hand motions: data-driven methods, and model-driven (data-free) methods. Data-driven methods map the relationship between human neural signals and wrist and hand motions through various machine learning methods, including classification, regression, and blind source separation. Davidge *et al.* proposed a linear discriminant analysis (LDA) method to classify combined wrist and hand motions, where both individual wrist or hand motions (single-DoF) and their combinations (muti-DoF) were labeled as different classes [1]. Despite the promising performance of this method, training samples from both single-DoF and multi-DoF motions were required to ensure a good classification performance. Parallel classification scheme [2], [3], linearly enhanced training [4], LDA dimensionality reduction [5], and muscle synergy analysis [6] were proposed to decompose complex classification tasks, by which simultaneous control of multi-DoF wrist and hand motions can be achieved through only single-DoF training. Yet, the number of DoFs that can be simultaneously controlled is limited and the classification performance is not ideal when the model is trained with only

Manuscript received 29 December 2021; revised 10 June 2022 and 19 July 2022; accepted 7 August 2022. Date of publication 10 August 2022; date of current version 8 September 2022. This work was supported in part by the National Natural Science Foundation of China under Grant 51575338 and Grant 61733011, in part by the Guangdong Science and Technology Research Council under Grant 2020B1515120064, and in part by the Shenzhen Science and Technology Program under Grant JCYJ20210324120214040. *(Corresponding authors: Honghai Liu; Pu Wang; Zhengen Zhao.)*

This work involved human subjects or animals in its research. Approval of all ethical and experimental procedures and protocols was granted by the SJTU Institutional Review Board under Application No. E2021103, and performed in line with the Declaration of Helsinki.

Xingchen Yang is with the Swiss Federal Institute of Technology Lausanne (EPFL), 1015 Lausanne, Switzerland (e-mail: xingchen.yang@epfl.ch).

Yifan Liu is with the State Key Laboratory of Robotics and Systems, Harbin Institute of Technology, Shenzhen 518055, China.

Zongtian Yin is with the Robotics Institute, Shanghai Jiao Tong University, Shanghai 200240, China.

Pu Wang is with the Seventh Affiliated Hospital, Sun Yat-sen University, Shenzhen 510275, China (e-mail: wangpu0816@qq.com).

Peilin Deng and Zhengen Zhao are with the Mianzhu People's Hospital, Mianzhu 618200, China (e-mail: mzzhengen@163.com).

Honghai Liu is with the State Key Laboratory of Robotics and Systems, Harbin Institute of Technology, Shenzhen 518055, China, and also with the School of Computing, University of Portsmouth, Portsmouth PO1 3HE, U.K. (e-mail: honghai.liu@icloud.com).

This article has supplementary downloadable material available at https://doi.org/10.1109/TNSRE.2022.3197875, provided by the authors.

Digital Object Identifier 10.1109/TNSRE.2022.3197875

single-DoF motions. In addition to classification methods, regression techniques have shown remarkable performance in the simultaneous prediction of multi-DoF wrist and hand motions. It can achieve a more natural proportional control of each DoF, albeit at the expense of increasing training complexity [7], [8], [9]. To reduce the training complexity while maintaining natural proportional control, Jiang *et al.* proposed a non-negative matrix factorization method to directly decode two-DoF wrist torques from surface electromyography (sEMG) [10]. This method can be used for simultaneous wrist and hand motion control but is usually limited to two-DoF control [11]. Recently, model-driven methods have been explored to overcome the complex training problems inherent to data-driven methods, where musculoskeletal models were applied to build the mapping between human neural signals and hand movements [12], [13]. Unfortunately, calibrating the parameters of musculoskeletal models remains troublesome. So far, complex training, limited controllable DoFs, and the lack of proportional control still limit the natural control of multi-DoF prosthetic hand.

In addition to intention recognition models, muscle sensing modalities play an important role in prosthetic control. Ultrasound sensing is an emerging modality in this field that can provide morphological information of functional muscles during hand movements. Compared to sEMG, it has a higher spatial resolution and can distinguish the activities of different muscles especially the deep-seated ones. Ultrasound has shown its ability in finger gesture recognition [14], [15], fingertip force estimation [16], lower limb motion recognition [17], gait phase identification [18], (virtual) prosthetic hand manipulation [19], [20], and soft exosuit control [21]. Moreover, our previous study demonstrated that simultaneous finger gestures and wrist rotation can be predicted by ultrasound sensing with a novel subclass discriminant analysis (SDA) algorithm [22]. This can achieve simultaneous control of multi-DoF wrist and hand motions with less user training time. However, the algorithm was only validated on non-disabled subjects, and the feasibility of ultrasound sensing in amputee prosthetic control remains to be verified, especially for simultaneous control of wrist and hand motions.

This paper seeks to explore the performance of wearable ultrasound on the simultaneous prediction of wrist and hand motions for amputees. We conducted an experiment to predict six finger gestures with concurrent wrist rotation (pronation/supination)[1] in four transradial amputees. As an extension to our previous study [22], we first validated the effectiveness of SDA on the simultaneous control of finger gestures and wrist rotation for amputees. Additionally, we proposed a novel multi-out Gaussian process (MOGP) model to achieve better control of simultaneous wrist and hand motions compared to SDA. Finally, we validated the potential of multi-task deep learning (MTDL) in further improving the performance of wrist and hand motion control. To promote the development of the prosthetic community, we will release the ultrasound-based adaptive prosthetic control dataset (UltraPro https://doi.org/10.6084/m9.figshare.20448489.v1). This paper will open up a new era of ultrasound-based prosthetic control.

[1]In this paper, unless otherwise specified, the wrist rotation refers to wrist pronation/supination.

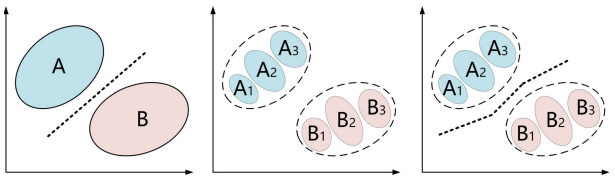

Fig. 1. Illustration of the subclass discriminant analysis (SDA), where original two classes (i.e., *A* and *B*) were divided into three subclasses (i.e., A_i and B_i). The classification of subclasses can give extra information about original classes and make the classification boundaries between original classes become non-linear.

II. Machine Learning Algorithms

The focus of this study is to achieve simultaneous prediction of different finger gestures and wrist rotation. To this end, we propose a series of algorithms that can accomplish different prediction tasks at the same time, including SDA, MOGP, and MTDL. We briefly summarize these algorithms as follows.

1) • Subclass Discriminant Analysis: SDA is an extension of LDA [23], which aims to solve non-Gaussian classification problems by separating classes at a subclass level, because the data distribution within a class can be a mixture of Gaussians [24]. By dividing each class into different subclasses that follow a Gaussian distribution, we can well describe the data variance of each class and obtain additional subclass information (Fig. 1). The research on SDA usually emphasize the separability of original classes rather than subclasses, ignoring the potential meaning of subclasses [25], [26], [27], [28]. Our previous study showed that the subclass information of each finger gesture can be used to represent the wrist rotation position [22]. Therefore, we can obtain simultaneous finger gesture and wrist rotation information by classifying finger gestures at a subclass level.

Supposing $C_i (i = 1, 2, \ldots, N)$ represents the data of finger gesture i, and $C_{ij} (j = 1, 2, \ldots, K)$ represents the subclass j of finger gesture i, and α represents the normalized wrist rotation angle of finger gesture i. By dividing the subclasses according to α, the subclass j can reflect the wrist rotation position. Taking three wrist rotation positions (i.e., wrist supination, wrist pronation, and neutral wrist position) as an example, the number of subclasses is set to 3 and the subdivision of each class is defined as follows

$$\begin{aligned} C_{i1} &: 0 \leq \alpha < l \\ C_{i2} &: l \leq \alpha < u \\ C_{i2} &: u \leq \alpha \leq 1 \end{aligned} \tag{1}$$

where l and u are hyperparameters for dividing wrist rotation positions. C_{i1}, C_{i2} and C_{i3} represent data from wrist supination, wrist pronation, and neutral wrist position, respectively. In terms of previous studies, α can be acquired by additional sensors like goniometer and inertial measurement unit (IMU) [22] or autonomous clustering methods [24], [25]. In addition, the first principal component (PC#1) of ultrasound features has been used to represent α, since the PC#1 is inherently linear to the wrist rotation angle [22]. In this study, we attempted IMU-, PC#1-, and Kmeans-based methods to obtain/cluster wrist rotation angles for the subclass division. For IMU- and PC#1-based methods, l and u were optimized with a dense grid search.

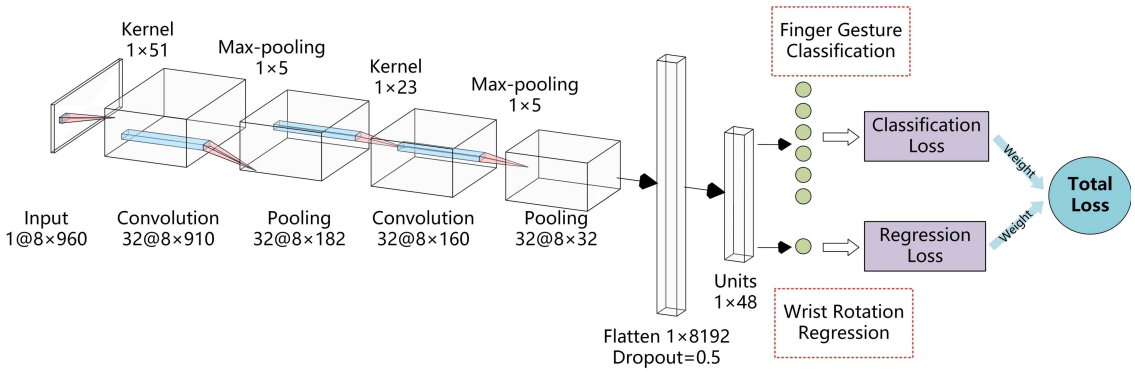

Fig. 2. Framework of the multi-task CNN model.

After dividing subclasses according to wrist rotation positions, we classify all subclasses together and then map the result ($C_{\overline{ij}}$) to finger gestures ($C_{\overline{ij}} \rightarrow C_{\overline{i}}$) and wrist rotation positions ($C_{\overline{ij}} \rightarrow C_{\overline{j}}$). Through this course-to-fine process, we can predict finger gestures and wrist rotation simultaneously.

2) • Muti-output Gaussian Process: Gaussian process (GP), a non-parametric Bayesian model, has shown excellent performance in hand kinematics prediction [29]. However, few have attempted the simultaneous prediction of multi-DoF wrist and hand motions using MOGP, especially for the mixed problems of classification and regression. Herein, we propose a MOGP model to achieve simultaneous prediction of discrete finger gestures (classification) and continuous wrist rotation (regression).

Define N training samples $X = \{x_n\}_{n=1}^{N}$ and corresponding targets $y = \{y_n\}_{n=1}^{N}$. (x_*, y_*) is a group of test sample. We can have a brief form of GP

$$\begin{bmatrix} y \\ y_* \end{bmatrix} \sim N\left(\begin{bmatrix} u \\ u_* \end{bmatrix}, \begin{bmatrix} K & K_*^T \\ K_* & K_{**} \end{bmatrix}\right) \tag{2}$$

where $\begin{bmatrix} u \\ u_* \end{bmatrix}$ is a mean vector and normally set to 0. K, K_*, K_{**} are kernel matrix of tranining data, kernel matrix between training data and test data, and kernel matrix of test data, respectively. The probability $p(y_*|y)$ also follows a Gaussian distribution

$$y_*|y \sim N\left(K_* K^{-1} y, K_{**} - K_* K^{-1} K_*^T\right) \tag{3}$$

The best estimation of y_* is

$$\hat{y}_* = K_* K^{-1} y \tag{4}$$

To achieve simultaneous prediction of finger gestures and wrist rotation, we define $y_n = (c_n, p_n)$, where c_n represents the finger gesture class and p_n represents the wrist rotation angle. To integrate classification and regression problems together, we convert c_n to one-hot encoding [30]. Therefore, $y_n = (one\text{-}hot(c_n), p_n)$, and the best estimation of y_* is

$$\hat{y}_* = K_* K^{-1}\{one\text{-}hot(c), p\} \tag{5}$$

Normally, the standard GP model assumes a single output variable only. To optimize the above-mentioned multi-output problem, we can build an independent GP for each output variable [31]. To improve computational efficiency, we attempted a batch independent multi-output GP (iMOGP) model, where kernel parameters are shared among different GPs.

Independent GP is a suboptimal solution for multi-output regression because the correlation among different output variables are not considered [31]. Considering the correlation between classification and regression tasks [32], we modify the kernel matrix K to

$$K_m = B \otimes K \tag{6}$$

$$B = \begin{pmatrix} b_{11} & b_{11} & \dots & b_{1T} \\ b_{21} & b_{22} & \dots & b_{2T} \\ \vdots & \vdots & \ddots & \vdots \\ b_{T1} & b_{T2} & \dots & b_{TT} \end{pmatrix} \tag{7}$$

where T represents the number of tasks, B_{ij} represents the correlation between different tasks, $\otimes$ represents Kronecker product.

In MOGP, the correlation between different tasks is usually considered, we therefore named it as general MOGP (gMOGP).

3) • Muti-task Deep Learning: Deep learning, represented by convolutional neural network (CNN) and autoencoder, has shown excellent performance in computer vision [33], natural language processing [34], and electrophysiological signal processing [35], because it can avoid tedious process of manually extracted features and has superior performance over traditional statistic learning models given enough data. As such, we propose a muti-task CNN (MTCNN) model for the simultaneous prediction of discrete finger gestures and continuous wrist rotation. The structure of the model is shown in Fig. 2, where $ReLU$ is used as activation function, cross entropy is used as classification loss function, and mean squared error is used as regression loss function. For both convolution and pooling, the stride step is set to one.

Unlike traditional single-output CNN models, the weights of our MTCNN model are shared among different tasks until the last fully connected layer, and the total loss is the weighted sum of the losses of different tasks [36].

$$loss_{total} = w loss_c + (1 - w) loss_r \tag{8}$$

where $loss_c$ is the loss of classification task, $loss_r$ is the loss of regression task, and w is the loss weight. w was optimized with a dense grid search ranging from 0 to 1, separated by 0.1, towards the aim of improving classification

TABLE I
AMPUTEE SUBJECT DEMOGRAPHICS

Subject	Age	Gender	Time since Amputation	Level of Amputation	Amputation Side	Prothesis Experience	Experiment Experience
A1	56	M	3 years	Transradial	Right	None	None
A2	71	M	15 years	Transradial	Right	None	None
A3	67	M	13 years	Transradial	Left	Cosmetic Prosthesis	Yes
A4	43	M	16 years	Transradial	Right	Myoelectric Prothesis	Yes

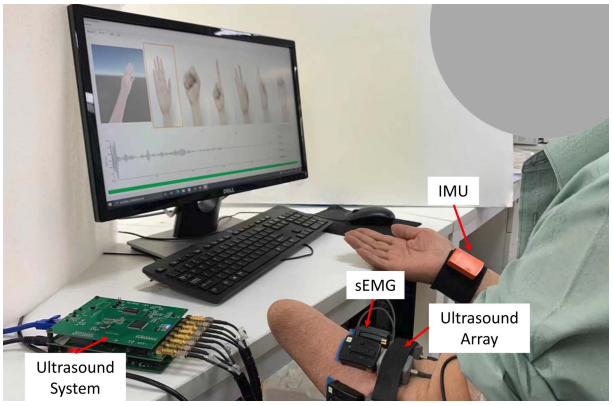

Fig. 3. Experiment setup. sEMG and IMU represent surface electromyography and inertial measurement unit, respectively.

performance of finger gestures. Because manually tuning the loss weight is a tedious and expensive process, we also attempt to select the loss weights of different tasks by considering the homoscedastic uncertainty of each task [37], where the loss balance of different tasks is addressed

$$loss_{total} = \frac{1}{2\sigma_1^2} loss_c + \frac{\gamma}{2\sigma_2^2} loss_r + \log(\sigma_1) + \log(\sigma_2) \quad (9)$$

where σ_1 and σ_2 are weight parameters that can be automatically learned by the CNN model. γ is a weight parameter used to balance the magnitude of $loss_c$ and $loss_f$. Empirically, γ is set as 10. When optimizing the weight parameters automatically, we name it as MTCNN-auto.

The implementation of SDA is based on Matlab 2016 Rb (Mathworks Inc.), and the implementation of MOGP and MTDL is based on Python with Pytorch framework.

III. EXPERIMENT EVALUATION

A. Data Recording

Four transradial amputees volunteered for this study. All provided the informed consent prior to participating in the experiment. The demographic information of the subjects is shown in Table I. The experiment was approved by the SJTU Institutional Review Board (E2021103).

The experiment setup is shown in Fig. 3. The subjects sat naturally, held their forearms horizontally, and kept palms upwards. The angle between the upper arm and the forearm was about 120°. Eight 5-MHz A-mode ultrasound transducers

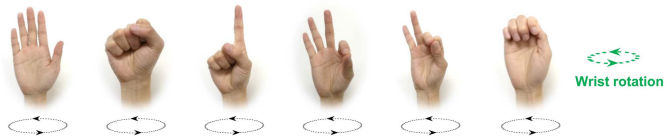

Fig. 4. Finger gestures. From left to right: rest (RS), power grip (PG), index point (IP), fine pinch (FP), tripod grip (TG), and key grip (KG).

were evenly attached around the forearm of the amputated side with a customized armband, and no specific muscle was targeted. The transducers were sequentially driven by a customized wearable ultrasound system, with a pulse repetition frequency (frame rate) of 10 Hz and sampling points of 1000 at 20 MHz sampling rate for each channel [20]. A commercial inertial measurement unit (IMU, Xsens-MTi-100, Xsens Technologies B.V., Netherlands) was attached on the wrist of the healthy side to measure wrist rotation angles. Eight sEMG sensors (TrignoTM Wireless System, Delsys Inc., Natick, MA, USA) were also evenly attached around the forearm near the ultrasound transducers. For A2, only seven sEMG sensors were attached due to the limited space. A custom-built software was used to stream ultrasound, sEMG and IMU signals synchronously to a computer. The sampling rate of the IMU sensor was set as 10 Hz to match the ultrasound data, and the sampling rate of sEMG was 1925.926 Hz.

Wrist rotation (pronation/supination) and six finger gestures were studied in this work, including rest (RS), fine pinch (FP), key grip (KG), tripod grip (TG), index point (IP), and power grip (PG) (Fig. 4). The subjects followed a dynamic mirrored bilateral training, in which they mimicked given movements simultaneously with both their intact and amputated hands. Movement of the intact hand is to assist the imaginary movement of the amputated hand [38]. Ultrasound and sEMG signals were collected from the amputated hand, and wrist rotation angles were collected from the intact hand. The experiment consisted of three repeated sessions. In each session, each finger gesture was performed for 50 seconds with concurrent wrist rotation at a frequency of approximately 0.5 Hz. Taking the neutral wrist position as 0°, the wrist rotation range was approximately −90° to 90°, i.e., from maximum pronation to maximum supination. To avoid muscle fatigue, there was 10 seconds of rest between two continuous finger gestures. Before formal data collection, subjects were given sufficient time to familiarize themselves with the experiment.

B. Data Processing

1) Ultrasound Feature Extraction: The mean value of a segment of A-mode ultrasound signal, which reflects the ultrasound echogenicity [17], was selected as the ultrasound feature. Specifically, the A-mode ultrasound signals were first preprocessed with time gain compensation, bandpass filtering, envelope detection, and log compression [14]. Then, the preprocessed ultrasound signals were evenly divided into a series of segments with a length of 20 data points. There were 1000 data points in each frame of ultrasound signal. Since the first and the last 20 data points carried little valuable information, they were removed before segmentation. Accordingly, the data of each sensing channel were divided into 48 segments. For each segment, the mean value (echogenicity) was extracted and noted as the feature. The features of different sensing channels were cascaded together, forming a 384×1 feature vector. Finally, principal component analysis was used to reduce the feature dimensionality, with 95% of the total variance preserved.

For deep learning method, the preprocessed ultrasound signals were directly input to the model.

2) sEMG Feature Extraction: The collected sEMG signals were first bandpass filtered between 20-450 Hz and comb filtered at 50Hz with Butterworth filters. Then, the filtered signals were segmented into 200 ms analysis windows with an overlap of 100 ms. Standard time domain feature sets were extracted from each analysis window, which consisted of mean absolute value (MAV), sign slope change (SSC), zero crossing (ZC), and waveform length (WL) [39]. Finally, the features from different channels were cascaded together.

3) Train-Test Split: We analyzed the data of each session individually. In each session, we collected 50 seconds of data for each finger gesture. To simulate the real-time application, the first 40 seconds of data of each finger gesture were split into the training set and the remaining into test set.

For deep learning method, the first 25% of data of each gesture in the test set was selected as validation set to optimize model hyperparameters, and the remaining was for testing. To give a fair comparison with the deep learning method, we recalculated the results of SDA and MOGP by discarding the validation set data when comparing with the CNN method.

4) Gesture Selection: For amputate subjects, the performed finger gestures were based on imaginations. This is highly dependent on their cognitive abilities, and confusion of some finger gestures is inevitable. To this end, we not only analyzed the prediction performance of all six gestures, but also evaluated the prediction performance of the best four or five gestures. During gesture selection, the gesture with the worst classification accuracy was removed.

C. Evaluation Metrics

We used classification accuracy to assess the finger gesture classification performance and coefficient of determination (R^2) to assess the wrist position prediction performance. Note that SDA can only predict discrete wrist rotation positions, so the wrist rotation prediction performance of SDA is assessed by classification accuracy.

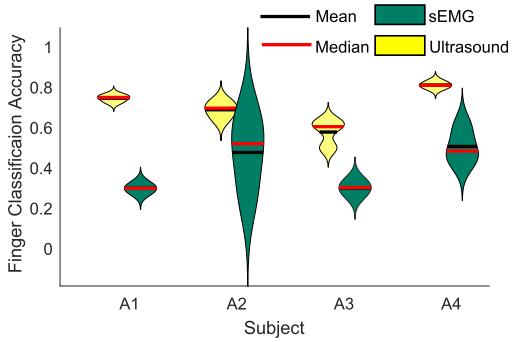

Fig. 5. Comparative analysis of sEMG and ultrasound on finger gesture classification.

D. Statistical Analysis

Two-way repeated-measure analysis of variance (ANOVA) followed by a Tukey post-hoc test was applied to evaluate the impact of different algorithms and subjects on the prediction performance. On the other hand, if analyzed data does not follow a normal distribution or does not meet the homogeneity of variance test, Mann-Whitney U test would be applied. The significance level was set to 0.05.

IV. Results

A. sEMG Vs. Ultrasound

The comparative analysis of sEMG and ultrasound on finger gesture classification is shown in Fig. 5, where the LDA classifier was applied. It was found that ultrasound outperformed sEMG significantly for all subjects, with higher classification accuracy and smaller standard deviation. Considering the poor finger gesture classification performance of sEMG in this experiment, only the results of ultrasound are reported below.

B. SDA

The performance of SDA for the simultaneous classification of wrist and hand motions is shown in Figs. 6(A) and (B), where LDA and quadratic discriminant analysis (QDA) are used as benchmarks. Statistical analysis shows that both algorithms and subjects have significant impacts on the classification performance, and there is no interaction between the two factors. For the finger gesture classification, the performance of SDA (e.g., SDA-IMU and SDA-PC#1) was significantly better than LDA and slightly better than QDA. In the meanwhile, SDA can achieve accurate classification of wrist rotation. Among different subclass division methods, SDA-PC#1 performed best, with a finger gesture classification accuracy of $74.78\% \pm 8.85\%$ and a wrist rotation classification accuracy of $92.5\% \pm 2.21\%$. Considering the superior performance of SDA-PC#1, we used SDA-PC#1 for the following comparative analyses.

The linear relationship between the normalized PC#1 and the normalized wrist rotation angle is shown in Fig. 7, and the detailed fitting metrics are listed in Table IV (highlighted in gray). This explains why the PC#1 of ultrasound features can be used for subclass division and also

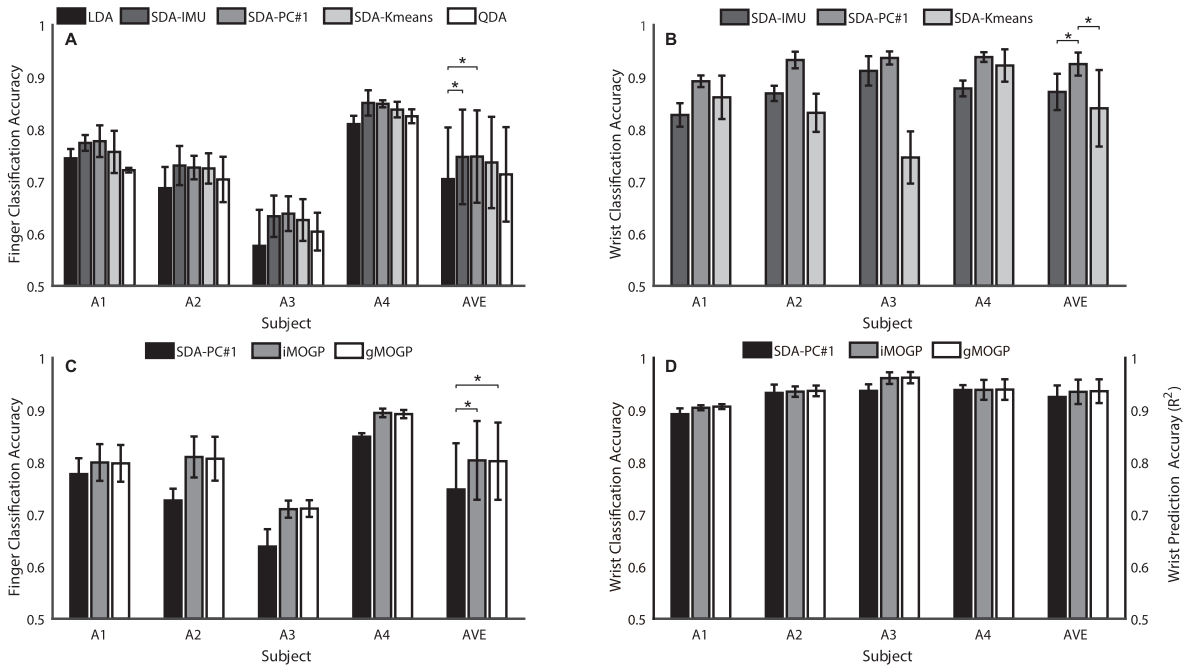

Fig. 6. Performance of simultaneous prediction of wrist and hand motions for different amputees. LDA: linear discriminant analysis, SDA: subclass discriminant analysis, QDA: quadratic discriminant analysis, iMOGP: batch independent multi-output Gaussian process, gMOGP: general multi-output Gaussian process. The standard deviations are shown with error bars, and the last column shows the average results of all subjects.

demonstrates the potential of PC#1 in continuous wrist rotation control.

C. MOGP

The performance of MOGP for the simultaneous prediction of wrist and hand motions is shown in Figs. 6 and (D), where SDA-PC#1 is used as a benchmark. Statistical analysis shows that both algorithms and subjects have significant impacts on the classification performance, and there is no interaction between the two factors. It was found that both iMOGP and gMOGP can significantly improve finger gesture classification performance, with a classification accuracy above 80%. At the meanwhile, MOGP (i.e., iMOGP and gMOGP) can accurately predict continuous wrist rotation positions, with a R^2 above 0.935. In addition, the performance of iMOGP was comparable to gMOGP. We did not compare the wrist rotation prediction performance of SDA and MOGP, since SDA was used for discrete wrist rotation classification while MOGP was used for continuous wrist rotation prediction. Considering the simplicity of iMOGP and its comparable performance to gMOGP, we used iMOGP for the following comparative analyses.

Fig. 8 shows the performance of SDA and MOGP for the simultaneous prediction of wrist and hand motions when the number of gestures is reduced from six to four. In terms of finger gesture classification, MOGP performed significantly better than SDA on the six or five gesture classification tasks, and slightly better than SDA on the four gesture classification task. Overall, when the number of gesture was reduced from six to four, the classification accuracy of MOGP increased from 80.35 ± 7.54% to 89.85 ± 4.27%. In terms of wrist rotation prediction, the performance of SDA remained stable

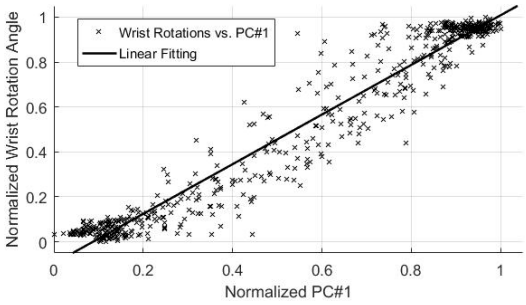

Fig. 7. Linear relationship between the normalized PC#1 of ultrasound features and the normalized wrist rotation angles for a representative subject.

TABLE II
GESTURES REMOVED WHEN REDUCING THE NUMBER OF GESTURES FROM SIX TO FOUR

Subject	Rem. Ges. 1	Rem. Ges. 2
A1	FP	KG
A2	KG	FP
A3	PG	FP
A4	FP	PG

while the performance of MOGP slightly decreased as the number of gestures reduced. Tables II shows the gestures removed when reducing the number of gestures from six to four ($Rem.Ges.i$ represents the ith removed gesture). FP, KG, and PG were usually removed during the gesture selection due to the similarity between FP and TG/RS and KG and PG.

Fig. 9 shows an example of the performance of MOGP on the simultaneous prediction of finger gestures and wrist

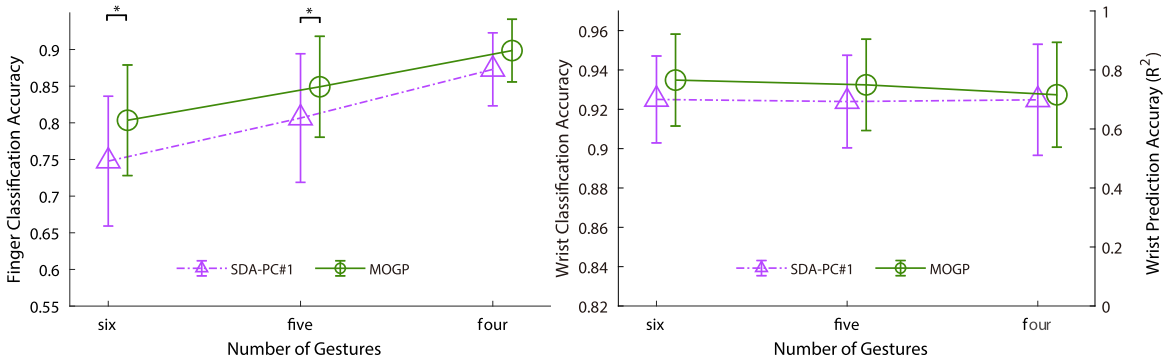

Fig. 8. Finger and wrist motion prediction performance when the number of finger gestures is reduced from six to four.

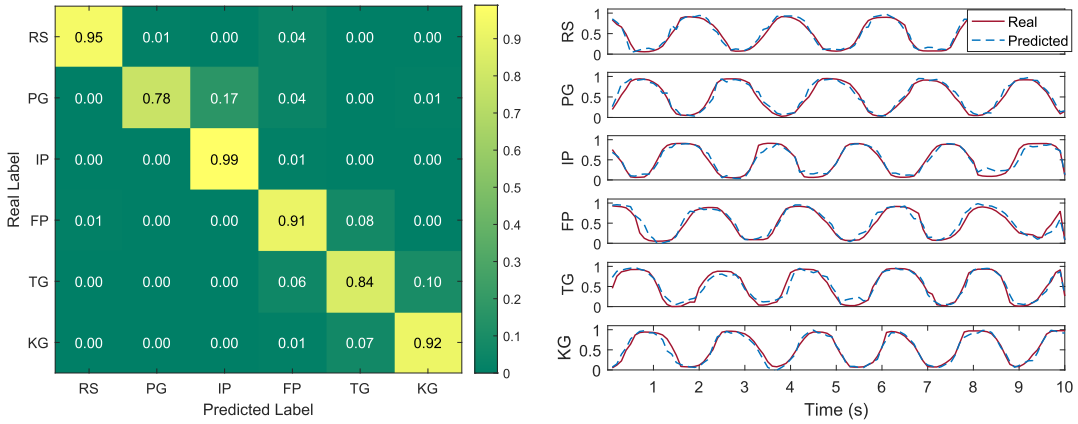

Fig. 9. Performance of MOGP on the simultaneous prediction of finger gestures and wrist rotaiton.

TABLE III
COMPARISON OF MOGP AND CNN ON FINGER GESTURE CLASSIFICATION (ACCURACY)

-	A_1-S_1	A_1-S_2	A_1-S_3	A_2-S_1	A_2-S_2	A_2-S_3	A_3-S_1	A_3-S_2	A_3-S_3	A_4-S_1	A_4-S_2	A_4-S_3
MOGP	0.764	0.84	0.749	**0.84**	**0.78**	0.74	**0.702**	**0.707**	0.667	0.887	**0.873**	0.862
CNN	0.76	0.827	0.764	0.829	0.764	0.8133	0.673	0.613	0.629	0.869	0.844	0.836
MTCNN-auto	0.753	0.831	0.764	0.82	0.74	0.802	0.691	0.609	0.656	0.876	0.836	**0.873**
MTCNN	**0.778**	**0.847**	**0.778**	**0.84**	**0.78**	**0.853**	**0.702**	0.676	**0.684**	**0.9**	0.853	0.871

rotation. Obviously, the finger gestures were accurately classified and the predicted wrist positions were well aligned with the real wrist positions.

D. MTDL

Fig. 10 shows the performance of MTDL for the simultaneous prediction of wrist and hand motions, where MOGP is used as a benchmark. Statistical analysis shows that only subjects have a significant impact on the classification performance, and there is no significant interaction between subjects and algorithms. Overall, the performance of MOGP, CNN, MTCNN, and MTCNN-auto were comparable for both finger gesture and wrist rotation prediction. The detailed results are listed in Tables III and IV (A_i-S_j represents data from *Amputee* i, *Session* j), where the best results were highlighted in bold. Despite no statistical difference, in most cases, MTCNN obtained the best finger gesture classification accuracy, and MOGP obtained the best wrist rotation prediction accuracy. With appropriate loss weights, MTCNN can always achieve better gesture classification accuracy than single-output CNN and in most cases achieve better gesture classification accuracy than MOGP (Table III), albeit at the expense of reducing accuracy of wrist rotation prediction (Table IV). MTCNN-auto can achieve a balanced performance between gesture classification and wrist rotation prediction.

In general, regression-based methods (i.e., MOGP, CNN, MTCNN, and MTCNN-auto) had better performance in wrist rotation prediction than the PC#1-based method.

V. DISCUSSION

Simultaneous prediction of wrist and hand motions with muscle signals is essential for the natural control of hand prostheses. sEMG has shown great potential in this field. It can represent neuromuscular activity and can be easily collected from the skin. However, due to the crosstalk, attenuation, and nonstationarity of sEMG signals, sEMG can only reflect

TABLE IV
COMPARISON OF MOGP AND CNN ON WRIST ROTATION PREDICTION (R^2)

-	A_1-S_1	A_1-S_2	A_1-S_3	A_2-S_1	A_2-S_2	A_2-S_3	A_3-S_1	A_3-S_2	A_3-S_3	A_4-S_1	A_4-S_2	A_4-S_3
PC#1	0.795	0.791	0.8	0.833	0.86	0.854	0.945	0.915	0.932	0.856	0.888	**0.874**
MOGP	**0.903**	**0.913**	**0.918**	**0.94**	**0.939**	**0.92**	0.963	0.914	**0.97**	**0.951**	**0.952**	0.804
CNN	0.876	0.922	0.892	0.934	0.932	0.906	**0.964**	**0.95**	0.967	0.95	0.947	0.8
MTCNN-auto	0.861	0.904	0.896	0.877	0.908	0.887	0.954	0.902	0.934	0.942	0.945	0.777
MTCNN	0.874	0.867	0.819	0.839	0.909	0.86	0.942	0.916	0.936	0.918	0.853	0.788

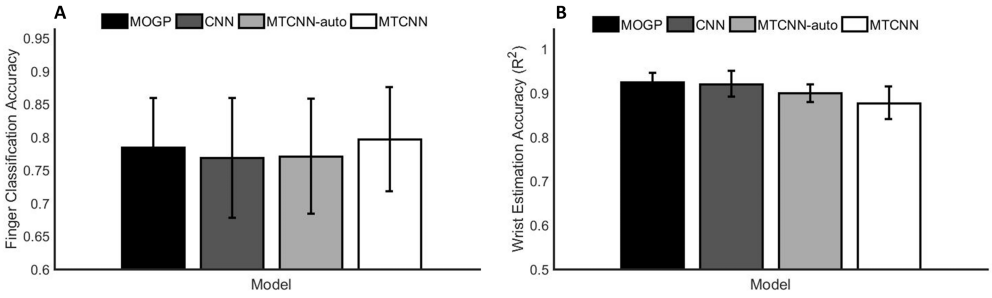

Fig. 10. Comparison of MOGP and CNN for the simultaneous prediction of wrist and hand motions.

activity of large and superficial muscles but cannot distinguish activity of finger- and wrist- related deep muscles. Therefore, the performance of sEMG on the simultaneous control of wrist and hand motions is limited [40]. Ultrasound can distinguish the activity of muscles centimeters below the skin, so it is able to decouple the movements of finger and wrist using morphological information of deep muscles [22]. To this end, we achieved simultaneous prediction of wrist and hand motions using ultrasound signals. To improve the useability of this technology, we applied a wearable A-mode ultrasound array instead of cumbersome B-mode ultrasound system. We have demonstrated that simultaneous finger gestures and wrist rotation can be predicted by ultrasound sensing with an SDA algorithm [22]. However, the algorithm was only validated in non-disabled subjects. In this study, for the first time, we validated the effectiveness of SDA in amputees. Additionally, in view of the limitations of traditional classification and regression techniques in simultaneous wrist and hand control - the training process is complex and the controllable DoFs are limited, we proposed a hybrid pattern recognition and regression scheme to achieve simultaneous control of multiple discrete finger gestures and continuous wrist rotation. Specifically, we proposed MOGP and MTDL to achieve this goal.

A. Effectiveness of SDA

In non-disabled subjects, we demonstrated that SDA can achieve accurate control of finger gestures and wrist rotation, and that SDA-PC#1 performed best among different subclass division methods. In addition, the performance of SDA was superior to LDA but inferior to QDA in finger gesture classification [22]. The results of our amputee test were highly consistent with the non-disabled test, except that QDA did not outperform SDA in gesture classification (Fig. 6A). This may arise from the difference of muscle condition between non-disabled and amputee subjects. Since the muscle contraction of amputees is significantly smaller than that of non-disabled subjects, the features of different finger gestures are mixed together and hard to be discriminated by simple quadratic classification boundaries. By contrast, SDA uses auxiliary supervision information from wrist rotation to classify finger gestures, so better classification boundaries can be found. To further verify the effectiveness of SDA, we divided the wrist rotation into one to five subclasses in turn. The subclasses were evenly divided according to the rotation range of the wrist. Results showed that SDA can robustly improve the finger gesture classification performance regardless of the subclass number (Fig. 11). When the number of subclasses was four, the best finger gesture classification performance can be achieved. The wrist classification performance decreased as the number of subclasses increased.

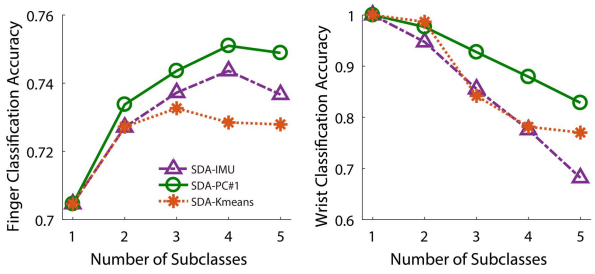

Fig. 11. Influence of subclass number on the classification performance of SDA.

Despite the remarkable performance of SDA, it can only control discrete wrist rotation. Our previous study showed that the PC#1 of ultrasound features was approximately linear to the wrist rotation position [22]. Therefore, it can be

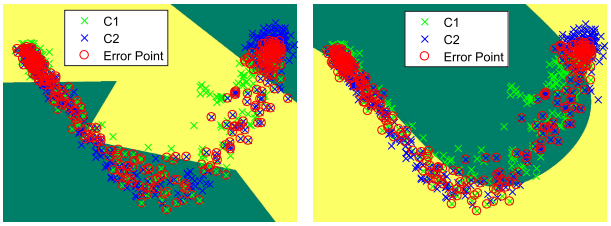

(a) SDA (b) MOGP

Fig. 12. Comparison of SDA and MOGP-based classification boundaries.

integrated into SDA for continuous wrist rotation control. Likewise, consistent results were obtained in our amputee test (Fig. 7 and Table IV).

B. Superiority of MOGP

While SDA and PC#1 are effective for wrist and hand motion control, the control performance remains to be improved. We applied GP here because it has shown excellent performance in hand kinematics prediction [41]. Instead of building individual GP model for gesture classification and wrist regression, a unified GP model for both tasks can reduce the computational burden. To this end, we converted the gesture classification task into a regression task using the one-hot encoding technology [30], so as to integrate it with the wrist regression task. Moreover, to take advantage of the inherent correlation between gesture classification and wrist regression tasks, we modified the kernel matrix to include the task correlation [32], [42]. Results showed that MOGP can significantly improve the performance of gesture classification and wrist rotation prediction compared to SDA and PC#1 (Fig. 6B), and the performance of iMOGP was comparable to gMOGP (Figs. 6C and 6D). One possible reason is that iMOGP has captured the inherent correlation between gesture classification and wrist regression when optimizing unified hyperparameters for the two tasks.

Fig. 12 shows a comparison of classification boundaries of SDA and MOGP. We found that both SDA and MOGP have the potential to solve the non-Gaussian classification problem. Here we did not find significant advantage of MOGP over SDA, because the features were reduced to two dimensions and the gesture classes were reduced to two. Nevertheless, the classification boundary of MOGP is a hypersurface, with better nonlinear characteristics than the hyperpolygonal boundary in SDA.

C. Potential of MTDL

In addition to MOGP, MTDL has been an effective way to solve multi-task prediction problems [36], [43]. Unlike extracting hand-crafted features and predicting them with a GP model, deep learning is a purely data-driven method that can achieve better performance given enough data. Previous studies have demonstrated that MTDL can achieve better performance than single-task models, because it can provide more supervision information for model training [37], [44]. In this study, we proposed an MTDL model and two optimization strategies to select the loss weights of different tasks. One is to manually optimize the loss weights of different tasks, and the other is to automatically optimize according to uncertainty [37]. When automatically optimizing the loss weights, the model can achieve a balanced performance between classification and regression, although both the accuracy of gesture classification and wrist regression were slightly lower than MOGP. When manually optimizing the loss weight towards the aim of improving gesture classification performance, the gesture classification accuracy of MTDL can exceed MOGP in most cases, albeit at the expense of reducing wrist rotation prediction accuracy. This demonstrated the potential of MTDL in further improving the gesture classification performance. Due to the limited amount of data, we only attempted simple one-dimensional convolution in this study. More complex CNN structures will be explored in the future.

D. Comparison of SDA, MOGP, and MTDL

Overall, MOGP and MTDL can achieve better performance in gesture classification and wrist rotation prediction. Nevertheless, SDA (i.e., SDA-PC#1) and PC#1 can achieve unsupervised prediction of wrist rotation. If the experiment platform is limited (e.g., in-home use), SDA and PC#1 will be good choices for wrist rotation control.

E. Comparison of sEMG and Ultrasound

To better present the gesture classification performance of ultrasound, we compared the gesture classification accuracy of ultrasound with currently prevailing sEMG (Fig. 5). Although there were differences in the placement of sEMG and ultrasound sensors, we found that ultrasound significantly outperformed sEMG on gesture classification accuracy. This result is consistent with our previous findings in non-disabled tests [45], further validating the potential of ultrasound in amputee prosthetic control. In our previous study [45], we also demonstrated that sEMG and ultrasound had complementary advantages, and indeed there have been several studies focusing on the fusion of sEMG and ultrasound for better motion intention prediction. Current fusions are typically limited to weighted averages of muscle activations obtained from sEMG and ultrasound [46] or cascades of sEMG and ultrasound features [47]. More fusion strategies should be explored to fully exploit the complementary information of the two signals.

F. Limitations and Future Work

First, gestures were held for a rather long time during the experiment, which is inconsistent with normal functional duration. Shortening the gesture hold time may result in unstable gesture classification performance due to transient muscle contractions during gesture switching. We will further evaluate the gesture classification performance in normal prosthetic functional tasks and use the major voting technique [48] to smooth the transient gesture classification results. Second, despite the promising results in this paper, we have not demonstrated how this simultaneous wrist and hand motion control strategy will improve the usability of functional prosthetic

hands compared to traditional pattern recognition control, and have not evaluated the cognitive demand of this new control strategy to amputees. These will be our future targets.

VI. Conclusion

In this study, we presented a novel MOGP algorithm and an MTDL model to achieve simultaneous prediction of finger gestures and wrist rotation for transradial amputees via wearable ultrasound sensing. Different from previous studies that focused on the classification or regression of combined wrist and hand motions, we proposed a hybrid pattern recognition and regression scheme to achieve simultaneous control of multiple discrete finger gestures and continuous wrist rotation. This can simplify user training and provide more controllable DoFs for simultaneous wrist and hand motion control. The results on four transradial amputees showed that the proposed MOGP can achieve accurate control of six types of finger gestures and wrist rotation, with better performance than previously reported SDA algorithm. Moreover, the MTDL has the potential to further improve the control performance. This paper validates the usability of ultrasound in the future prosthetic hand control.

Acknowledgment

The authors would like to thank the Shanghai Jiao Tong University (SJTU) postdoctoral fellowship council for their support.

References

[1] K. Davidge, "Multifunction myoelectric control using a linear electrode array," Ph.D. dissertation, Dept. Elect. Comput. Eng., Univ. New Brunswick, Fredericton, ON, Canada, 2005.

[2] A. J. Young, L. H. Smith, E. J. Rouse, and L. J. Hargrove, "A new hierarchical approach for simultaneous control of multi-joint powered prostheses," in *Proc. 4th IEEE RAS EMBS Int. Conf. Biomed. Robot. Biomechatronics (BioRob)*, Jun. 2012, pp. 514–520.

[3] A. J. Young, L. H. Smith, E. J. Rouse, and L. J. Hargrove, "Classification of simultaneous movements using surface EMG pattern recognition," *IEEE Trans. Biomed. Eng.*, vol. 60, no. 5, pp. 1250–1258, May 2013.

[4] M. Nowak and C. Castellini, "The LET procedure for prosthetic myocontrol: Towards multi-DOF control using single-DOF activations," *PLoS ONE*, vol. 11, no. 9, Sep. 2016, Art. no. e0161678.

[5] C. W. Antuvan and L. Masia, "An LDA-based approach for real-time simultaneous classification of movements using surface electromyography," *IEEE Trans. Neural Syst. Rehabil. Eng.*, vol. 27, no. 3, pp. 552–561, Mar. 2019.

[6] A. Furui *et al.*, "A myoelectric prosthetic hand with muscle synergy–based motion determination and impedance model–based biomimetic control," *Sci. Robot.*, vol. 4, no. 31, 2019, Art. no. eaaw6339.

[7] S. Muceli and D. Farina, "Simultaneous and proportional estimation of hand kinematics from EMG during mirrored movements at multiple degrees-of-freedom," *IEEE Trans. Neural Syst. Rehabil. Eng.*, vol. 20, no. 3, pp. 371–378, May 2012.

[8] J. M. Hahne *et al.*, "Linear and nonlinear regression techniques for simultaneous and proportional myoelectric control," *IEEE Trans. Neural Syst. Rehabil. Eng.*, vol. 22, no. 2, pp. 269–279, Mar. 2014.

[9] J. M. Hahne, M. A. Schweisfurth, M. Koppe, and D. Farina, "Simultaneous control of multiple functions of bionic hand prostheses: Performance and robustness in end users," *Sci. Robot.*, vol. 3, no. 19, Jun. 2018.

[10] N. Jiang, K. B. Englehart, and P. A. Parker, "Extracting simultaneous and proportional neural control information for multiple-dof prostheses from the surface electromyographic signal," *IEEE Trans. Biomed. Eng.*, vol. 56, no. 4, pp. 1070–1080, Apr. 2009.

[11] C. Chen, Y. Yu, X. Sheng, D. Farina, and X. Zhu, "Simultaneous and proportional control of wrist and hand movements by decoding motor unit discharges in real time," *J. Neural Eng.*, vol. 18, no. 5, Oct. 2021, Art. no. 056010.

[12] L. Pan, D. L. Crouch, and H. Huang, "Myoelectric control based on a generic musculoskeletal model: Toward a multi-user neural-machine interface," *IEEE Trans. Neural Syst. Rehabil. Eng.*, vol. 26, no. 7, pp. 1435–1442, Jul. 2018.

[13] E. Zheng, J. Wan, L. Yang, Q. Wang, and H. Qiao, "Wrist angle estimation with a musculoskeletal model driven by electrical impedance tomography signals," *IEEE Robot. Autom. Lett.*, vol. 6, no. 2, pp. 2186–2193, Apr. 2021.

[14] X. Yang, X. Sun, D. Zhou, Y. Li, and H. Liu, "Towards wearable a-mode ultrasound sensing for real-time finger motion recognition," *IEEE Trans. Neural Syst. Rehabil. Eng.*, vol. 26, no. 6, pp. 1199–1208, Jun. 2018.

[15] C. Castellini, G. Passig, and E. Zarka, "Using ultrasound images of the forearm to predict finger positions," *IEEE Trans. Neural Syst. Rehabil. Eng.*, vol. 20, no. 6, pp. 788–797, Nov. 2012.

[16] D. S. González and C. Catellini, "A realistic implementation of ultrasound imaging as a human-machine interface for upper-limb amputees," *Front. Neurorobot.*, vol. 7, p. 17, Oct. 2013.

[17] M. H. Jahanandish, N. P. Fey, and K. Hoyt, "Lower limb motion estimation using ultrasound imaging: A framework for assistive device control," *IEEE J. Biomed. Health Inform.*, vol. 23, no. 6, pp. 2505–2514, Nov. 2019.

[18] M. H. Jahanandish, K. G. Rabe, N. P. Fey, and K. Hoyt, "Gait phase identification during level, incline and decline ambulation tasks using portable sonomyographic sensing," in *Proc. IEEE 16th Int. Conf. Rehabil. Robot. (ICORR)*, Jun. 2019, pp. 988–993.

[19] C. A. Baker, N. Akhlaghi, H. Rangwala, J. Kosecka, and S. Sikdar, "Real-time, ultrasound-based control of a virtual hand by a trans-radial amputee," in *Proc. 38th Annu. Int. Conf. IEEE Eng. Med. Biol. Soc. (EMBC)*, Aug. 2016, pp. 3219–3222.

[20] X. Yang, Z. Chen, N. Hettiarachchi, J. Yan, and H. Liu, "A wearable ultrasound system for sensing muscular morphological deformations," *IEEE Trans. Syst., Man, Cybern., Syst.*, vol. 51, no. 6, pp. 3370–3379, Jun. 2021.

[21] R. W. Nuckols, S. Lee, K. Swaminathan, D. Orzel, R. D. Howe, and C. J. Walsh, "Individualization of exosuit assistance based on measured muscle dynamics during versatile walking," *Sci. Robot.*, vol. 6, no. 60, Nov. 2021, Art. no. eabj1362.

[22] X. Yang, J. Yan, Y. Fang, D. Zhou, and H. Liu, "Simultaneous prediction of wrist/hand motion via wearable ultrasound sensing," *IEEE Trans. Neural Syst. Rehabil. Eng.*, vol. 28, no. 4, pp. 970–977, Apr. 2020.

[23] S. Balakrishnama and A. Ganapathiraju, "Linear discriminant analysis—A brief tutorial," *Inst. Signal Inf. Process.*, vol. 18, pp. 1–8, Mar. 1998.

[24] M. Zhu and A. M. Martínez, "Subclass discriminant analysis," *IEEE Trans. Pattern Anal. Mach. Intell.*, vol. 28, no. 8, pp. 1274–1286, Aug. 2006.

[25] N. Gkalelis, V. Mezaris, and I. Kompatsiaris, "Mixture subclass discriminant analysis," *IEEE Signal Process. Lett.*, vol. 18, no. 5, pp. 319–322, May 2011.

[26] H. Wan, H. Wang, G. Guo, and X. Wei, "Separability-oriented subclass discriminant analysis," *IEEE Trans. Pattern Anal. Mach. Intell.*, vol. 40, no. 2, pp. 409–422, Feb. 2018.

[27] F. Oveisi, "Subclass discriminant analysis using dynamic cluster formation for EEG-based brain-computer interface," in *Proc. 4th Int. IEEE/EMBS Conf. Neural Eng.*, Apr. 2009, pp. 303–306.

[28] M. Zhu and A. M. Martinez, "Optimal subclass discovery for discriminant analysis," in *Proc. Conf. Comput. Vis. Pattern Recognit. Workshop*, Jun./Jul. 2004, p. 97.

[29] J. G. Ngeo, T. Tamei, and T. Shibata, "Continuous and simultaneous estimation of finger kinematics using inputs from an EMG-to-muscle activation model," *J. Neuroeng. Rehabil.*, vol. 11, no. 1, pp. 1–14, 2014.

[30] J. Li, Y. Si, T. Xu, and S. Jiang, "Deep convolutional neural network based ECG classification system using information fusion and one-hot encoding techniques," *Math. Problems Eng.*, vol. 2018, Dec. 2018, Art. no. 7354081.

[31] L. Yang, K. Wang, and L. Mihaylova, "Online sparse multi-output Gaussian process regression and learning," *IEEE Trans. Signal Inf. Process. Over Netw.*, vol. 5, no. 2, pp. 258–272, Jun. 2019.

[32] C. Williams, E. V. Bonilla, and K. M. Chai, "Multi-task Gaussian process prediction," in *Proc. Adv. Neural Inf. Process. Syst.*, 2007, pp. 153–160.

[33] A. Voulodimos, N. Doulamis, A. Doulamis, and E. Protopapadakis, "Deep learning for computer vision: A brief review," *Comput. Intell. Neurosci.*, vol. 2018, Feb. 2018, Art. no. 7068349.

[34] T. Young, D. Hazarika, S. Poria, and E. Cambria, "Recent trends in deep learning based natural language processing," *IEEE Comput. Intell. Mag.*, vol. 13, no. 3, pp. 55–75, Aug. 2018.

[35] Y. Yu, C. Chen, J. Zhao, X. Sheng, and X. Zhu, "Surface electromyography image-driven torque estimation of multi-DoF wrist movements," *IEEE Trans. Ind. Electron.*, vol. 69, no. 1, pp. 795–804, Jan. 2022.

[36] Q. Gao, S. Jiang, and P. B. Shull, "Simultaneous hand gesture classification and finger angle estimation via a novel dual-output deep learning model," *Sensors*, vol. 20, no. 10, p. 2972, May 2020.

[37] R. Cipolla, Y. Gal, and A. Kendall, "Multi-task learning using uncertainty to weigh losses for scene geometry and semantics," in *Proc. IEEE/CVF Conf. Comput. Vis. Pattern Recognit.*, Jun. 2018, pp. 7482–7491.

[38] J. L. Nielsen, S. Holmgaard, N. Jiang, K. B. Englehart, D. Farina, and P. A. Parker, "Simultaneous and proportional force estimation for multifunction myoelectric prostheses using mirrored bilateral training," *IEEE Trans. Biomed. Eng.*, vol. 58, no. 3, pp. 681–688, Mar. 2011.

[39] B. Hudgins, P. Parker, and R. N. Scott, "A new strategy for multifunction myoelectric control," *IEEE Trans. Biomed. Eng.*, vol. 40, no. 1, pp. 82–94, Jan. 1993.

[40] X. Yang, Y. Zhou, and H. Liu, "Wearable ultrasound-based decoding of simultaneous wrist/hand kinematics," *IEEE Trans. Ind. Electron.*, vol. 68, no. 9, pp. 8667–8675, Sep. 2021.

[41] Q. Zhang, T. Pi, R. Liu, and C. Xiong, "Simultaneous and proportional estimation of multijoint kinematics from EMG signals for myocontrol of robotic hands," *IEEE/ASME Trans. Mechatronics*, vol. 25, no. 4, pp. 1953–1960, Aug. 2020.

[42] P. Moreno-Muñoz, A. Artés-Rodríguez, and M. A. Álvarez, "Heterogeneous multi-output Gaussian process prediction," 2018, *arXiv:1805.07633*.

[43] D. Luvizon, D. Picard, and H. Tabia, "Multi-task deep learning for real-time 3D human pose estimation and action recognition," *IEEE Trans. Pattern Anal. Mach. Intell.*, vol. 43, no. 8, pp. 2752–2764, Aug. 2021.

[44] Y. Zhang and Q. Yang, "A survey on multi-task learning," 2017, *arXiv:1707.08114*.

[45] X. Yang, J. Yan, and H. Liu, "Comparative analysis of wearable a-mode ultrasound and sEMG for muscle-computer interface," *IEEE Trans. Biomed. Eng.*, vol. 67, no. 9, pp. 2434–2442, Sep. 2020.

[46] Q. Zhang, K. Kim, and N. Sharma, "Prediction of ankle dorsiflexion moment by combined ultrasound sonography and electromyography," *IEEE Trans. Neural Syst. Rehabil. Eng.*, vol. 28, no. 1, pp. 318–327, Jan. 2020.

[47] Q. Zhang, W. H. Clark, J. R. Franz, and N. Sharma, "Personalized fusion of ultrasound and electromyography-derived neuromuscular features increases prediction accuracy of ankle moment during plantarflexion," *Biomed. Signal Process. Control*, vol. 71, Jan. 2022, Art. no. 103100.

[48] W. Geng, Y. Du, W. Jin, W. Wei, Y. Hu, and J. Li, "Gesture recognition by instantaneous surface EMG images," *Sci. Rep.*, vol. 6, no. 1, pp. 1–8, Dec. 2016.